Osteoblast Adhesion on Poly(L-lactic Acid)/Polystyrene Demixed Thin Film Blends: Effect of Nanotopography, Surface Chemistry, and Wettability

Jung Yul Lim,[†] Joshua C. Hansen,[‡] Christopher A. Siedlecki,[‡,§] Robert W. Hengstebeck,[||] Juan Cheng,[⊥] Nicholas Winograd,[⊥] and Henry J. Donahue*,[†]

Division of Musculoskeletal Sciences, Department of Orthopaedics and Rehabilitation, Center for Biomedical Devices and Functional Tissue Engineering, Department of Bioengineering, and Department of Surgery, College of Medicine, Pennsylvania State University, Hershey, Pennsylvania 17033, and Materials Research Institute and Department of Chemistry, Pennsylvania State University, University Park, Pennsylvania 16802

Received May 19, 2005; Revised Manuscript Received August 8, 2005

Biomaterial surface characteristics are critical cues that regulate cell function. We produced a novel series of poly(L-lactic acid) (PLLA) and polystyrene demixed nanotopographic films to provide nonbiological cell-stimulating cues. The increase in PLLA weight fraction (ϕ) in blend solutions resulted in topography changes in spin-cast films from pit-dominant to island-dominant morphologies having nanoscale depth or height (3−29 nm). Lower molecular weight PLLA segregated to the top surface of demixed films, as observed by X-ray photoelectron spectroscopy and secondary ion mass spectroscopy (SIMS). For $\phi \geq 0.5$, the topmost film layer was predominantly filled with PLLA (>96% by SIMS at 20-Å depth). Nanotextured substrata stimulated osteoblastic cell adhesion to a greater degree than did flat PLLA ($\phi = 1$), and this effect was more pronounced for nanoisland ($\phi = 0.7$ and 0.9) relative to nanopit topographies ($\phi = 0.5$). Demixed films having relatively lower water contact angles generally enhanced cell adhesion and spreading. Our results reveal that cell adhesion is affected by surface chemistry, topography, and wettability simultaneously and that nanotextured surfaces may be utilized in regulating cell adhesion.

Introduction

Biomaterials science and tissue engineering have been focusing on what characteristic cues induce cells to behave in a controlled and predictable manner. The control of cell behavior may focus on various aspects, e.g., preferential adherence to specific substrates, variable cell migration, degree of cell-to-cell communication, rate of proliferation, time-dependent expression of specific cell phenotype, and responsiveness to extracellular signals. The development of biomaterials having individual, purpose-specific cues that can stimulate cells to behave in a predictable manner and in a predetermined time course would have tremendous benefit to tissue engineering. For example, such biomaterials could be used to control the multipotent capability of stem cells.[1,2]

One critical category of cell-stimulating cues is biomaterial characteristics.[3−5] When cells adhere and grow on substrates, cells sense, interpret, and integrate extracellular signals and respond to them. Thus, chemical and physical signals from biomaterial surfaces, e.g., surface chemistry, topography, charge, energy, and wettability, are critical extracellular stimulators that have the potential to regulate cell behavior. We have investigated substrate surface energy and nanotopography effects on osteoblastic cell behavior and observed that subtle changes in wettability or nanotopographic feature scale can induce substantial variances in osteoblastic cell adhesion, spreading, focal adhesive integrin $\alpha v\beta 3$ and vinculin protein expression, proliferation, gene expression, and cell sheet detachment.[6−10]

Studies on substratum topography effects have shown that cells display differential behavior depending on the topographic "scale" and "feature". For example, anisotropic micro- or nanometer scale ridges and grooves have been shown to induce contact-guided cell alignment in the anisotropic direction.[11−13] This contact guidance was positively correlated with focal contact formation and cytoskeletal organization.[14,15] Another topographic feature potentially affecting cell behavior is isotropic micro- or nanometer scale topographies that have evenly or randomly distributed features (pits, islands, holes, etc.) throughout the substrate surface.[10,16−23] Most of studies examining isotropic features, including our own previous work,[10] have focused on differential cell responses, such as adhesion and differentiation, as a function of topographic scale, including nanoscale island height. These studies aim to develop cell-adhesive or nonadhesive substrates depending on the topographic scale.

* Corresponding author. Henry J. Donahue, Department of Orthopaedics and Rehabilitation, College of Medicine, Pennsylvania State University, 500 University Drive, Hershey, PA 17033. Phone: (717) 531-4809. Fax: (717) 531-7583. E-mail: hdonahue@psu.edu.

[†] Department of Orthopaedics and Rehabilitation.

[‡] Department of Bioengineering.

[§] Department of Surgery.

[||] Materials Research Institute.

[⊥] Department of Chemistry.

10.1021/bm0503423 CCC: $30.25
Published on Web 00/00/0000

Topographic scale is an important biomimic regulator of cell behavior, and nanotopography may be even more relevant to the biomimicry concept than microtopography. This is because cells in vivo exist in topographic interfaces closer to the nanometer scale than to the micrometer scale, e.g., the 20−200-nm feltlike topography of human cornea basement membrane,[13] the cross-striation pattern every 67 nm of type I collagen,[24] and the 10 nm thick fibrils and 20 nm pores of rat kidney membrane.[25] Nanofabrication techniques, including electron beam lithography (10 nm), colloidal particle adsorption (5 nm), microcontact printing (200 nm), and self-organizing or self-assembling systems (10 nm), have expanded cell-substratum interaction studies to the nanometer range.[26] Polymer demixing techniques, one of the self-organizing systems, utilize polymeric phase separation during a critical high-speed spin-casting process. Phase separation using slightly immiscible polymer blends[10,16−21] or diblock copolymers[27,28] results in a rise of topographic features of ca. 10−100 nm scale. This technique can control the topographic features (pits, ribbons, or islands in case of blends; spheres, lamellae, cylinders, or bicontinuous in case of copolymers) by varying the polymer composition or copolymer structure and the size of a particular feature by varying the concentration of the spin-casting solution.

In this study, using a series of poly(L-lactic acid) (PLLA) and polystyrene (PS) blends, we produced novel nanotopographic substrates of demixed thin films having pit or island topographies of nanoscale depth or height. Topography of the demixed films was assessed by atomic force microscopy (AFM), while film surface chemistry was examined by X-ray photoelectron spectroscopy (XPS) and secondary ion mass spectroscopy (SIMS). These films varied in topography (pits or islands), surface chemistry (PLLA segregating to the top surface), and resultant wettability. As regards polymeric phase separation and selective PLLA air interface segregation, we described interplay between molecular weight and surface energy of component polymers in the demixing process. The film substrates constituted a unique set of samples by which we could compare cell response with respect to various nonbiological cell-stimulating cues (chemistry, topography, and wettability) individually or collectively. We report in this study preliminary cytocompatibility results of short-term osteoblastic cell adhesion and spreading.

Experimental Section

Spin-Casting of PLLA/PS Blend Films. Thin film substrates having randomly distributed topographic features were produced by PLLA/PS polymer demixing. PLLA ($M_w = 50 \times 10^3$) and PS ($M_w = 289 \times 10^3$) were purchased from Polysciences (Warrington, PA) and Aldrich Chemical Co. (Milwaukee, WI), respectively. A series of PLLA/PS mixtures (0/100, 10/90, 30/70, 50/50, 70/30, 90/10, and 100/0 w/w) were dissolved in chloroform to have a total polymer concentration of 1% w/w. PLLA weight fraction in the spin-casting solution is noted as ϕ in this study ($\phi = 0$, 0.1, 0.3, 0.5, ..., 1). Spin-casting of polymer solutions onto glass cover slips was performed at 4000 rpm for 30 s using a Spin-coater (Specialty Coating Systems, Indianapolis, IN). Spin-cast films were dried at room temperature with no annealing. For sterilization, film substrata were treated under ultra-violet light for 1 h before cell culture.

Film Surface Characterization. AFM. Topography of demixed PLLA/PS and control PLLA and PS films was observed using AFM (Nanoscope IIIa, Digital Instruments, Santa Barbara, CA). Measurements were done in tapping mode under ambient conditions using silicon tips (Mikro-Masch). For each substratum, three samples were each examined at three random spots. Height or depth of topographic features was estimated by the cross-sectional analysis. The percentage of the raised feature area was quantified by subtracting the fraction of pits (in case of pit topography) or sea portion (in case of island topography). "ImageJ" image analysis software was used to set the threshold for a bump or a pit on two-dimensional height images obtained from the AFM. Film thickness was assessed by AFM after removing a portion of the film manually.

XPS. The spin-cast films were characterized by an Axis Ultra (Kratos Analytical) using monochromatic Al Kα X-rays (1486.7 eV) with samples oriented normal to the entrance lens of the spectrometer. The binding energy linearity and instrumental transmission function were calibrated from reference spectra collected for Cu, Ag, and Au metal foils for the lens settings used in this analysis. Survey scans and high-resolution scans of the C1s and O1s peaks were acquired at two spots per sample film. The surface composition was quantified by applying the appropriate relative sensitivity factors (RSFs) and transmission function to the integral peak area of C1s and O1s peaks. The RSFs take into account the X-ray cross section and inelastic mean free path (λ). The sampling depth defined as 3λ of the C1s line was approximately 90 Å in this study. Sample charging was minimized with low-energy electrons (< 5 eV) through the minimization of the full width at half maximum (fwhm) of the C1s and O1s peaks. The demixed films and pure PS films were charge referenced to the aromatic benzyl C peak of PS at 284.76 eV.[29] For the pure PLLA films, the XPS spectra were charge-referenced to the methyl C peak of PLLA at 285 eV.[29]

SIMS. Chemical composition of the topmost surface layer of the spin-cast films was characterized by SIMS equipped with a time-of-flight (TOF) detector system. The TOF-SIMS instrumentation is described in detail elsewhere[30] and summarized briefly below. The instrument is equipped with an Au primary ion source (Ionoptika, Southampton, UK) which is directed at a 40° angle relative to the substrate surface. The source was operated at an anode voltage of 25 kV. The pulsed primary Au^+ beam (50 ns and ca. 1 nA) was rastered across a $200 \times 200\ \mu m^2$ area. The total ion dose was always less than 10^{12} ions/cm^2. Signal intensity was determined from the integrated peak area for each specific peak and was obtained as averages over three measurements. Charge compensation was not necessary for any of the samples examined. Under these conditions, SIMS measurements were estimated to give an approximate sampling depth of 20 Å.

Contact Angle Measurements. Wettability of test films was assessed by measuring water contact angle (θ) using a G10 contact angle instrument (KRÜSS, Hamburg, Germany).

Table 1. Topography of PLLA/PS Demixed Thin Film Blends (Mean ± Standard Deviation)

PLLA/PS weight fraction in blend solution (ϕ)	topography	depth of pits or height of islands (nm)	area of pits or islands (μm^2)	coverage of raised features (%)
PS (0)				
10/90 (0.1)	pits	2.8 ± 0.8	0.01 ± 0.002	73.4 ± 1.7
30/70 (0.3)	pits	16.9 ± 4.8	0.18 ± 0.044	70.2 ± 2.7
50/50 (0.5)	pits	28.5 ± 4.3	0.18 ± 0.039	67.9 ± 1.9
70/30 (0.7)	islands	21.0 ± 4.7	0.06 ± 0.015	36.3 ± 1.3
90/10 (0.9)	islands	9.0 ± 1.9	0.01 ± 0.006	35.0 ± 4.0
PLLA (1)				

Double-distilled water was gently dropped on test films and static contact angle was monitored after 0 and 5 min. Means and standard deviations from five measurements are reported.

Cytocompatibility Assays. Cell Area. Human fetal osteoblastic (hFOB 1.19, hFOB) cells were subcultured in Dulbecco's modified Eagle's medium (DMEM)-Ham's F-12 1:1 medium (GIBCO, Grand Island, NY) supplemented with 10% (v/v) fetal bovine serum (FBS, HyClone, Logan, UT), and 1% (v/v) penicillin−streptomycin on tissue culture PS (TCPS) dishes and incubated at 37 °C in a standard incubator with 5% CO_2 in air. Prior to cell culture assays, cells were routinely removed from TCPS by rinsing in phosphate buffered saline (PBS) and incubating in trypsin−ethylenediaminetetraacetic acid solution. For assessing cell morphology, cells were seeded on test substrata at 1.3×10^4 cells/cm^2 using the same complete media. After culturing 3 h, substrates were washed with PBS and attached cells were fixed with paraformaldehyde solution in PBS (4% w/v) for 20 min. Fixed cells were stained for 2 min using 0.5% w/v Coomassie blue aqueous solution containing methanol/glacial acetic acid, washed with distilled water, and observed using a Nikon OPTIPHOT-2 optical transmission microscope. Five random spot images of $960 \times 720\ \mu m^2$ size, each containing 25−50 cells, were obtained at a 10× objective magnification (under 10× eyepieces) from repeated cell culture experiments. By use of ImageJ, cell outlines were detected and cell area was calculated based on the number of pixels covered by the cell, and means and standard deviations are reported. Cells clustered with each other were excluded from data sets and a total of 100−300 cells per substrata were analyzed.

Cell Adhesion. For adhesion assays, cells were cultured by the same method described above and allowed to adhere to each substratum. After 3 h, nonadherent cells were removed by washing with PBS three times and the attached cell number was determined by trypsinization and hemacytometer counting. Adhesion assays were performed three times, each in triplicate. Average adhesion percentages and standard deviations are reported.

Statistics. Statistical significance between groups was assessed by one-way analysis of variance (ANOVA) followed by Student-Newman-Keuls post-hoc multiple comparison tests. Comparisons with a flat PS control (*, $p < 0.05$; **, $p < 0.01$) and a flat PLLA control ($^{\#}$, $p < 0.05$; $^{\#\#}$, $p < 0.01$) are presented.

Results

Topography of PLLA/PS Demixed Films. PLLA/PS demixed films at 1% w/w spin-casting solution concentration displayed nm scale textured surfaces (in feature depth or height, Table 1), while PLLA or PS single component spin-cast films had flat surfaces (Figure 1, each shown at different maximum heights). The texture of demixed films was altered by varying the blend composition. Demixed films from blend solutions with a lower PLLA dose ($\phi \leq 0.5$) displayed a topography composed of mostly interconnected, randomly distributed pits (parts b−d of Figure 1), while those from higher ϕ ($\phi \geq 0.7$) displayed a randomly distributed island

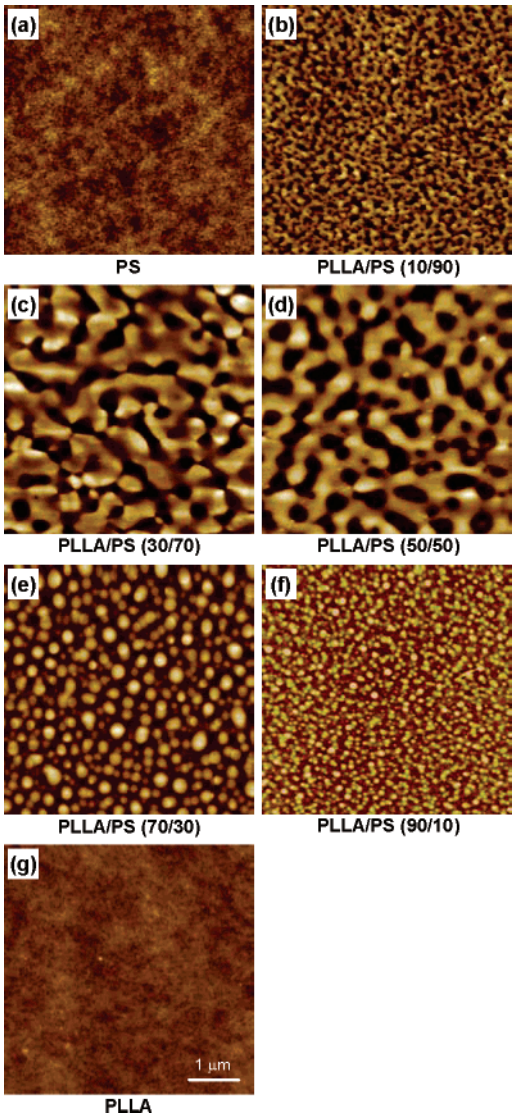

Figure 1. AFM images of PLLA/PS demixed thin film blends spin-cast at various polymer compositions (w/w) and pure component films. $5 \times 5\ \mu m^2$ size images are shown at different *z*-axis maximum heights of 3 nm (a), 5 nm (b), 25 nm (c), 40 nm (d), 45 nm (e), 15 nm (f), and 5 nm (g). The brighter color represents the higher portion.

topography (parts e and f of Figure 1). These topographies are referred to as pit- or island-dominant topographies, respectively. The depth of pits or height of islands was small (≤10 nm) for blend films at low or high ϕ (0.1 and 0.9), while they were relatively large (17−29 nm) at intermediate ϕ (Table 1). Between the two island-dominant topographies, the island height was relatively larger at $\phi = 0.7$ than at $\phi = 0.9$. With regards to the topography coverage, PS content appears to influence the percentage area covered by the raised features (Table 1). However, the correlation between the two displayed large deviations at some compositions. Among pit-dominant topographies, blend films at $\phi = 0.3$ and 0.5 displayed similar pit area and similar percentage surface coverage. The two island dominant topographies ($\phi = 0.7$ and 0.9) displayed different island area but similar percentage surface coverage. The actual surface area of textured substrata including sidewalls of pits or islands was not assessed. Thickness of test films was in the range of ca. 70−80 nm.

XPS Analysis. The elements present in the survey scans of the demixed films and pure PLLA films were C and O but only C in the case of pure PS films. To calculate the chemical composition, high-resolution scans were curve fit using the constraints determined from the high-resolution spectra of the pure PS and PLLA films. In the high-resolution C1s spectra of pure PS, the primary C1s peak at ca. 285 eV is composed of two components from the aromatic ring at 284.76 eV (C^a in Figure 2b where italic superscripts denote C atoms in the structural formulas) and the aliphatic backbone at 285 eV (C^b in Figure 2b) with a peak area ratio of 6:2.[29] This gives an area constraint of $[C^a] = 3 \times [C^b]$, where [] implies a peak area. PS also has a series of $\pi-\pi^*$ shake-up peaks at ca. 292 eV.[29,31] The combined contribution of the satellite peaks represented 9.2% of the total C1s peak area similar to the reference data.[29] The PS contribution to the C1s peak was determined such that the binding energy of the aliphatic and satellite components were linear offsets of the primary aromatic C and that the fwhm and peak area contributions were considered as direct scalars of the aromatic C. Each contribution could thus be added to calculate the PS contribution to the C1s spectra as in eq 1

$$[C_{PS}] = [C^a] + [C^b] + [C^{satellite}] \quad (1)$$

The average relative concentration ratio of C to O in the pure PLLA films was 3.1:1.9, which is consistent with the expected ratio of 3:2 given by the molecular structure (Figure 2b) and with the reference data.[29] High-resolution C1s spectra of the pure PLLA films displayed three peaks of equal intensity at 285, 286.97, and 289.04 eV (Figure 2a) each corresponding to three C atoms (C^c, C^d, and C^e) in the PLLA repeating unit, as is consistent with the reference.[29] This sets an area constraint of $[C^c] = [C^d] = [C^e]$. Figure 2a shows a continuous change from PS to PLLA specific characteristics in high-resolution C1s spectra. However, components of the PLLA differentially charge shifted from the PS components by 0.55 eV for all of the demixed films. These shifts were used as constraints in the curve fitting of the C1s spectra of the demixed films. To fully account for PLLA contribution, one must account for the contribution from O. A simple

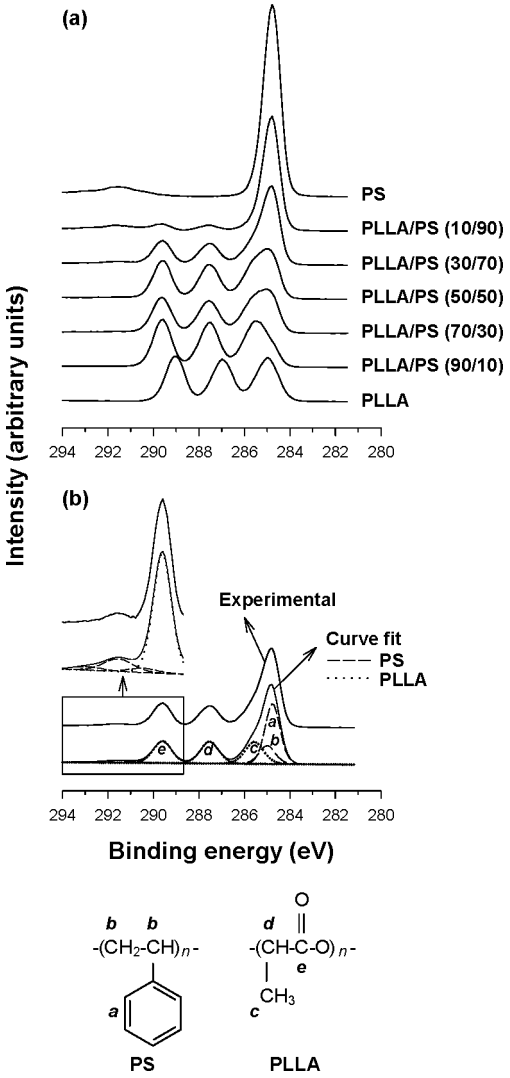

Figure 2. (a) High-resolution C1s XPS spectra of PLLA/PS demixed thin film blends spin-cast at various polymer compositions (w/w) and pure component films. For clarity, spectra of all test films are shown together by making *y*-axis shifts in their XPS intensities. (b) Curve fit example is shown for the experimental C1s XPS spectra of PLLA/PS (30/70 w/w) demixed films. Curve fit spectrum with PS (C^a and C^b) and PLLA (C^c, C^d, and C^e) specific component peaks is shown, where italic superscripts denote C atoms in the structural formulas. Satellite peak at ca. 292 eV was also counted in PS contribution calculations as is shown in magnified graph.

approach is to adjust the added PLLA specific peak area based on the structural formula

$$5/3[C_{PLLA}] = 5/3([C^c] + [C^d] + [C^e]) \quad (2)$$

This takes into account the contribution from the two O atoms of PLLA. Finally, the film surface PLLA fraction ($\Phi_{XPS,PLLA}$) was calculated as in eq 3

$$\Phi_{XPS,PLLA} = 5/3[C_{PLLA}]/([C_{PS}] + 5/3[C_{PLLA}]) \quad (3)$$

O1s spectra (not shown) were also used to calculate the surface composition. Briefly, the film surface PLLA fraction was calculated as the ratio of the curve-fit intensity of PLLA component to the intensity of a pure PLLA standard. This is shown as "XPS (Oxygen)" data in Figure 4 together with "XPS (Carbon)" data explained above.

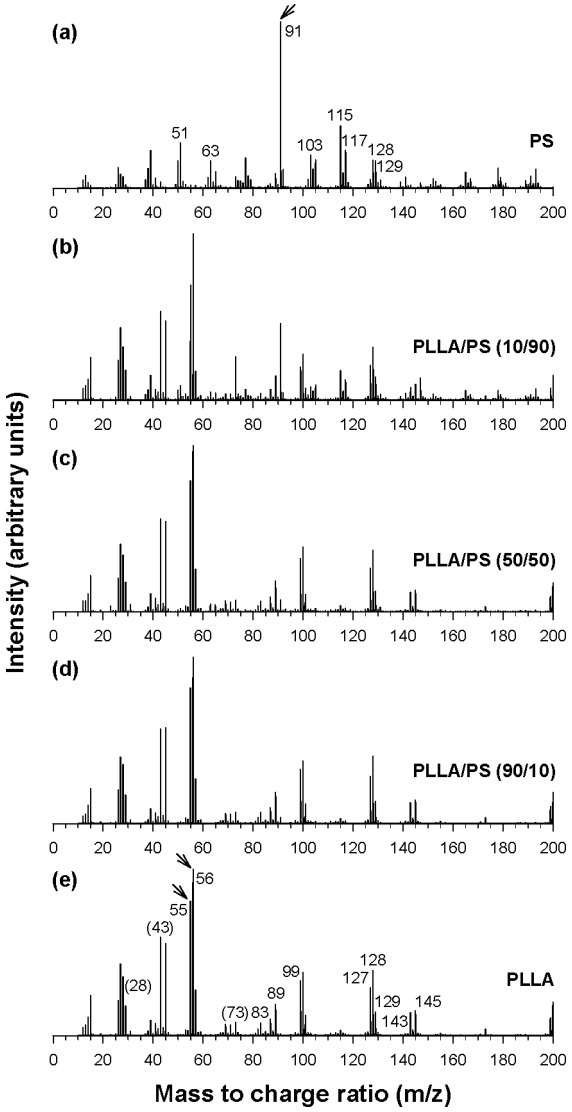

Figure 3. Positive SIMS spectra of PLLA/PS demixed thin film blends spin-cast at various polymer compositions (w/w) and pure component films. Spectra are shown at different maximum intensity counts of 655 (a), 1388 (b), 5289 (c), 5442 (d), and 5062 (e). PS and PLLA specific peaks are noted in parts a and e, respectively, and characteristic peaks used in composition calculation are noted by arrows. Poly(dimethylsiloxane) contamination peaks were detected on PLLA-containing films at positions shown in parentheses.

SIMS Analysis. Positive-ion SIMS spectra in the low-mass range ($m/z = 0-200$) revealed a drastic change from PS to PLLA specific secondary ion detections (Figure 3 shown at different maximum counts). In SIMS spectra of pure PS, various PS characteristic fragments were detected, i.e., $m/z = 51$, 63, 91, 103, 115, 117, 128, and 129. With increasing ϕ, PS specific peaks were dramatically attenuated and PLLA specific peaks appeared, i.e., $m/z = 43$, 55, 56, 73, 83, 89, 99, 127, 128, 129, 143, and 145. These PS and PLLA peaks are consistent with references, and the suggested fragment structure can be found in the literature.[32−34] For films displaying a PLLA component, contamination peaks from poly(dimethylsiloxane) were detected at $m/z = 28$, 43, and 73 (43 and 73 peaks are superimposed on PLLA peaks). They were not observed on pure PS films. This contamination on pure PLLA films was also reported by Mahoney et al.,[33] but it is not clear from where this originates.

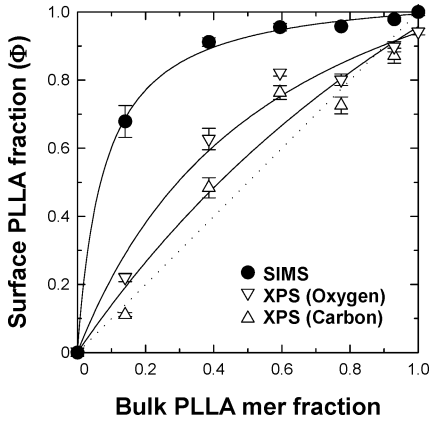

Figure 4. Plot of film surface PLLA fraction (Φ) vs bulk PLLA fraction in the blend solution (see text for *x*-axis presentation). Results from C1s- and O1s-based XPS measurements and SIMS data are shown with regression lines. Dotted line is an equivalent composition line.

SIMS peaks for composition calculation were chosen among the peaks listed above, using the criteria that peaks should exhibit PS or PLLA specific characteristic at higher detection counts but not be detected in the SIMS spectra of the other pure polymer. Three peaks fulfilled these criteria (arrows in Figure 3), i.e., the peak at $m/z = 91$ for PS produced by a $C_7H_7^+$ fragment and peaks at 55 and 56 for PLLA from $C_3H_3O^+$ and $C_3H_4O^+$ fragments, respectively. The PLLA composition in the spin-cast film surface ($\Phi_{SIMS,PLLA}$) was calculated as below

$$\Phi_{SIMS,PLLA} = [C_3H_3O^+]/([C_7H_7^+] + [C_3H_3O^+]) \text{ or } [C_3H_4O^+]/([C_7H_7^+] + [C_3H_4O^+]) \quad (4)$$

These two fraction values were averaged and presented in Figure 4 as SIMS data.

Surface Chemistry of PLLA/PS Demixed Films. Quantitative XPS and SIMS data are assembled in Figure 4, which is shown with the *x* axis of a fractional amount of PLLA repeating unit in the blend solution. It was obtained by dividing the weight fraction ratio (w/w) of the two polymers by the molecular weight of the repeating unit of each polymer, i.e., 71.05 and 104.15 atomic mass unit for PLLA and PS, respectively. For example, PLLA/PS = 50/50 sample ($\phi = 0.5$) yields (50/71.05):(50/104.15) = 0.59:0.41, and data are plotted at an *x* axis value of 0.59. This plot is more relevant, when comparing bulk and film surface compositions than a plot using the *x* axis of a nominal PLLA weight fraction (ϕ). For clarity, however, we will continue to use the nominal weight fraction (ϕ) in the following sections.

Most of the XPS and SIMS data and their three regression lines are located above the dotted equivalent composition line. This implies that the PLLA fraction in the demixed film surface is greater than the bulk PLLA fraction in the spin-casting solution. In other words, PLLA components tend to segregate to the top surface of the demixed films. Furthermore, the degree of PLLA segregation differed as a function of the depth from an air−film interface, as is confirmed by XPS and SIMS data. Recalling that the sampling depth is different for the two techniques, it can be concluded that PLLA enrichment in the film surface is more severe at an

Table 2. Water Contact Angle of PLLA/PS Demixed Thin Film Blends

PLLA/PS weight fraction in blend solution (ϕ)	contact angle (degree)	
	0 min	5 min
PS (0)	81.6 ± 0.8	81.1 ± 0.7
10/90 (0.1)	73.9 ± 1.4	69.6 ± 1.3
30/70 (0.3)	68.6 ± 1.2	64.2 ± 1.0
50/50 (0.5)	65.0 ± 0.9	61.0 ± 1.2
70/30 (0.7)	63.4 ± 0.9	58.5 ± 1.1
90/10 (0.9)	63.0 ± 1.3	57.7 ± 1.4
PLLA (1)	63.8 ± 1.0	61.9 ± 1.0

air−film interface layer (as assessed by SIMS at 20 Å depth) than at deeper layers (as assessed by XPS at 90 Å depth). We note again that these sampling depths of XPS and SIMS are both approximate values and that they are not usually defined in the same way. However, it is certain that SIMS represents much shallower layers, in other words, the topmost film surface layers. We also note that SIMS results in Figure 4 were obtained by assuming relative SIMS sensitivities of all fragments to be equal. SIMS spectra displayed a large increase in PLLA signal compared to the PS signal at an air−film interface (Figure 3), and even a large disparity in sensitivities would not alter the dominance of the PLLA segments at the film surface. The comparison of XPS data from C1s- or O1s-based calculations may provide additional evidence for PLLA surface segregation tendency in that the PLLA film surface fraction from the O1s calculation is slightly larger than that from the C1s calculation. Because of the PLLA segregation to the air interface, demixed films at PLLA doses of $\phi \geq 0.5$ (x axis value ≥ 0.59) may be inferred to exhibit topmost layers filled primarily with PLLA composition (>96% by SIMS). This suggests that, in a reasonable error range (<5%), the four test substrata at $\phi =$ 0.5, 0.7, 0.9, and 1 can be regarded as having the same topmost surface chemistry of PLLA.

Wettability of PLLA/PS Demixed Films. Both PS and PLLA are rather hydrophobic polymers, as shown by larger water contact angles (Table 2). Contact angles of test substrata measured at the time of water-drop deposition (0 min) decreased from 82° for relatively more hydrophobic PS to 64° for relatively less hydrophobic PLLA. The decrease in θ with increasing PLLA content was rapid at the lower PLLA dose range ($\phi \leq 0.5$) and then saturated to similar contact angles (ca. 63−65°) at the higher PLLA dose range ($\phi \geq 0.5$), a trend relevant to SIMS surface chemistry. When measured after 5 min, contact angles of demixed, textured substrata decreased by 4−5°, while flat pure PS and PLLA controls remained similar. This demonstrates a topography-induced wettability change when substratum roughness is impregnated by measurement water. As a result, island textured films at $\phi = 0.7$ and 0.9 displayed lower θ at 5 min than flat films at $\phi = 1$.

hFOB Cell Adhesion and Spreading on PLLA/PS Demixed Films. In Coomassie blue stained images, cells cultured on demixed films at $\phi = 0.7$ and 0.9 (parts e and f of Figure 5) displayed higher cell attachment and more cell spreading. On PS and PLLA flat control films, cells were less spread out and often stellate shaped. The quantified adhered cell area at 3 h of culture is shown in Figure 6a.

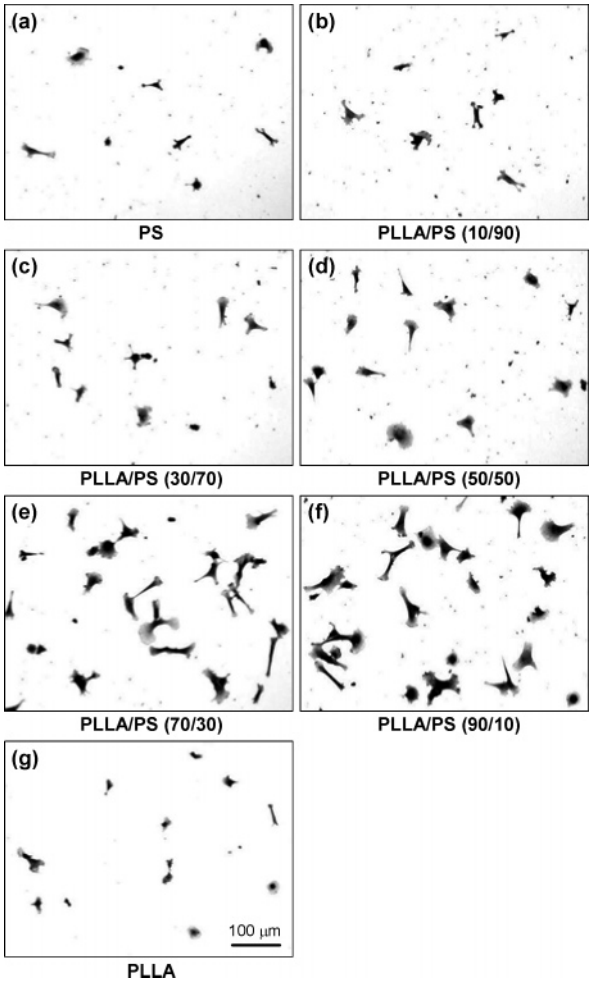

Figure 5. Optical microscope images of Coomassie blue stained cells cultured for 3 h on PLLA/PS demixed thin film blends spin-cast at various polymer compositions (w/w) and pure component films. Original 960 × 720 μm^2 size images were taken and used for image analysis, while cropped sample images (600 × 450 μm^2) are shown with a scale bar.

Cells on PLLA enriched, island textured films ($\phi = 0.7$ and 0.9) exhibited a significantly larger cell area than cells on PS and PLLA flat controls. Cell area on the other textured surfaces was not significantly different.

Cell adhesion percentage was sensitive to changes in surface characteristics of polymer demixed films (Figure 6b presented together with surface characteristics described in previous sections). hFOB cell adhesion was generally higher on PLLA surface-enriched substrata ($\phi \geq 0.5$) than on surfaces having a PS component ($\phi < 0.5$). Cells on PS flat films showed a little lower adhesion than did cells on PLLA flat films. The substratum topography effect could be assessed under reasonably similar surface chemical compositions, i.e., substrata at $0.5 \leq \phi \leq 1$ whose topmost layers are filled mostly with PLLA (by SIMS). Nanotextured substrata ($\phi = 0.5$, 0.7, and 0.9) induced significantly greater cell adhesion than did flat PLLA control ($\phi = 1$). This effect was more pronounced for nanoisland topography ($\phi = 0.7$ and 0.9) relative to nanopit topography ($\phi = 0.5$). Though cell adhesion on the two island topographies was not statistically different, the average was a little higher for films at $\phi = 0.9$ having relatively smaller nanoisland height (see Table 1). Among the three pit topographies, cell adhesion

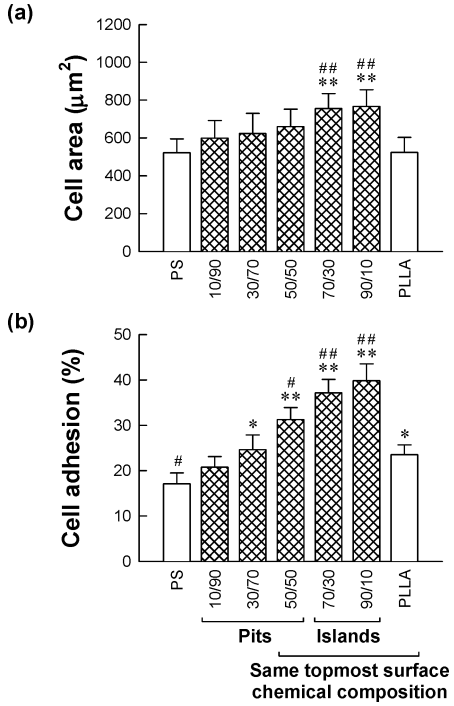

Figure 6. hFOB cell area (a) and degree of adhesion (b) at 3 h of culture on PLLA/PS demixed thin film blends spin-cast at various polymer compositions (w/w) and pure component films. Statistical significance assessed by ANOVA followed by Student−Newman−Keuls post-hoc tests is shown as * ($p < 0.05$) and ** ($p < 0.01$) when compared with a flat PS control and # ($p < 0.05$) and ## ($p < 0.01$) when compared with a flat PLLA control. Corresponding substratum surface characteristics are also noted. Under the same topmost surface layer chemistry ($0.5 \leq \phi \leq 1$) observed by SIMS, cell adhesion is enhanced on nanotextured surfaces. This effect was more pronounced for nanoisland topography ($\phi = 0.7$ and 0.9) relative to nanopit topography ($\phi = 0.5$).

was greater on films at $\phi = 0.5$ that had greater PLLA surface enrichment. As regards the effect of substratum wettability, cell adhesion was generally lower on relatively more hydrophobic substrata (compare Table 2 with Figure 6b). The wettability of textured surfaces, however, did not always correlate with cell adhesion, e.g., cell adhesion on demixed films at $\phi = 0.5$ was greater than that on flat controls ($\phi = 1$) while the two substrata displayed similar wettability.

Discussion

We produced a novel series of PLLA/PS demixed nanotopographic substrates differing in topography, surface chemistry, and wettability. Pit- or island-dominant topographies in nanometer-scale depth or height were produced, and PLLA predominantly segregated to the air interface of the demixed films. Nanotextured surfaces stimulated greater cell adhesion and spreading than did flat control films. In comparison with nanotexture effects, the chemistry difference between PLLA and PS flat films displayed a less significant effect on cell adhesion and spreading. Wettability of demixed films displayed a positive correlation with short-term cytocompatibility. We demonstrated that biomaterial characteristics are interdependent and short-term cell behavior is affected by these parameters simultaneously and competitively.

Polymeric phase separation determines composition variation in polymer thin film blends. Surface topography is formed during phase separation and aggregation. Various factors affect this "self-organizing" system, e.g., compatibilities, surface energies, and molecular weights of component polymers.[35−40] If the component polymers are less compatible, the degree of phase separation is generally more severe. Polymer segregation to the air interface is a complex interplay between surface energy and molecular weight.[38] It has been reported that lower surface energy components tend to segregate at the air−polymer interface of demixed films in order to minimize the magnitude of interfacial free energy, e.g., deuterated PS (dPS) in PS/dPS,[41] poly(vinyl methyl ether) (PVME) in PS/PVME,[42] and poly(butyl methacrylate) (PBMA) in PS/PBMA.[43] However, a contrary observation was reported for high molecular weight PS/low molecular weight poly(methyl methacrylate) (PMMA) blend films in which the high surface energy component of PMMA segregated at the air interface.[38] Polymer chains at the air interface will have restricted chain conformations and thus smaller conformational entropy compared with chains in the deeper bulk region of the film. Thus, the film surface may be favorably covered by the low molecular weight component, as longer polymer chains at the surface may suffer a severe conformational entropic penalty.[38]

Knowing which component polymer segregates to the air interface is important when assessing cell behavior, as cells will see only the topmost layer of the test substrata. PLLA/PS demixing developed in this study may belong to the case of high molecular weight PS/low molecular weight PMMA blend films described above, which unexpectedly displayed a high surface energy component segregated to the air interface. PLLA has a slightly higher surface energy than PS, which is indirectly confirmed by the lower θ of pure PLLA relative to pure PS (Table 2). Water adhesion tension (τ) of test surfaces calculated by θ ($\tau = \gamma \cos \theta$, $\gamma = 72.8$ dyn/cm: water surface tension) has been used as a relative measure of surface energy of test surfaces.[4,6−10] The Owens's method, which quantifies surface energy by combining two contact angle measurements of water and methylene iodine,[44] is also a relative estimation which does not give an absolute value. In any method, higher surface energy surfaces generate lower contact angles. Therefore, our XPS and SIMS results demonstrating the higher surface energy component (PLLA) segregating to the air interface suggest that the surface energy effect was overcome by the molecular weight derived entropy effect. In other words, relatively lower molecular weight PLLA ($M_w = 50 \times 10^3$) segregated to the air−film interface, irrespective of its relatively higher surface energy to reduce an entropic penalty that may arise when relatively high molecular weight PS ($M_w = 289 \times 10^3$) is exposed to air interface.

By combining XPS and SIMS data with AFM results, phase separation and aggregation in vertical and lateral axes may be proposed. The percentage of raised feature area at the film surface, as assessed by AFM, was more related to the amount of the PS bulk content in the blend solution than the PLLA bulk content (Table 1). This suggests that the raised features may be mostly composed of aggregated PS

segments. On the other hand, SIMS revealed strong PLLA segregation to the air−film interface. If combined, PLLA/PS demixed films at 70/30 w/w ($\phi = 0.7$) would have randomly distributed PS aggregated islands that are embedded in a PLLA matrix and are also top covered by a surface segregated PLLA thin (20 Å) layer. The film structure may be further assessed as a function of each spatial axis via dynamic SIMS,[33] selective etching technique,[45] etc.

Recently, cellular response to nanotopography has been examined using polymer demixed substrata.[10,16−21] On PS/poly(4-bromostyrene) (PBrS)[17−19] and PS/PBMA[20] demixed films, fibroblasts displayed differential adhesion and focal adhesion protein synthesis as a function of topographic feature height (13−95 nm). We demonstrated that osteoblastic cells sense and react to PS/PBrS demixed nanotopography having 11, 38, and 85 nm high islands not only in adhesion-related cell behavior but also in bone cell phenotype.[10] While these studies have focused on nanotopographic scale by varying blend solution concentrations, we focused on topographic features by varying blend compositions. One advantage of the PLLA/PS demixing is that as demixed films at $0.5 \leq \phi \leq 1$ may be considered to have the same topmost layer chemistry, due to the severe PLLA surface segregation, the topography effect could be assessed without being hampered by the different chemistry. In addition, as PLLA is one of the more widely used biopolymers, films enriched with PLLA in the topmost layer may be more end-purpose relevant substrates for bioengineering applications than PS or PBMA surface segregated films.[16−21]

One important finding in this study is that nanotextured surfaces stimulate osteoblastic cell adhesion, and this was more distinct for nanoisland relative to nanopit topographies (Figure 6b). Cell adhesion on the two nanoisland textures was a little higher at $\phi = 0.9$ with relatively smaller island height (9 nm) than at $\phi = 0.7$ with relatively larger island height (21 nm) (Table 1), though not statistically different. This trend is generally consistent with our previous results, i.e., hFOB adhesion on PS/PBrS demixed islands decreases significantly with increasing island height (11 > 38 > 85 nm).[10] Topographic scale difference between films at $\phi = 0.7$ and 0.9 appears not to be sufficient to cause a significant difference in cell adhesion. In comparison of pit and island topographies, the more pronounced effect of the nanoisland texture on cell adhesion might be due to the total area difference including sidewalls or the different coarseness of texture. It is assumed that finer topographic features and larger total area of islands may contribute to the enhanced cell adhesion, which is, however, not clear.

We also found that various biomaterial characteristics are intercorrelated. For instance, bulk chemical composition in blend solution affects topography via phase separation and aggregation, resulting in film surface chemistry variation. Additionally, wettability of demixed films was altered by film surface chemistry and topography. Short-term cytocompatibility was positively correlated with surface wettability, similar to previous reports showing greater cell adhesion and spreading on more hydrophilic surfaces.[3−10] However, the finding that substrate wettability was not always closely correlated with cell adhesion (e.g., different adhesion but similar wettability for films at $\phi = 0.5$ and 1) suggests that substrate characteristics other than wettability play an independent role in stimulating cell behavior. Furthermore, nanotextured surfaces induced greater cell adhesion than flat controls. These observations indicate that, when assessing cell response, various biomaterial characteristics should be assessed individually and collectively. Additionally, effects of substrate surface characteristics on protein adsorption should also be considered,[46−48] as this will in turn affect cell behavior.[3,5,10] Our results suggest that topography modification in nm scale may be exploited in regulating cell function in various bioengineering areas including tissue engineering. For example, widely recognized lower cell adhesion on hydrophobic PLLA may be improved via nanotopographic surface fabrication.

In summary, PLLA/PS demixed thin film blends were produced having pit or island topographies in nanometer scale depth or height. The strong PLLA air−interface segregation made it possible to assess the substrate topography effect exclusively. We demonstrated that cell adhesion was affected by various interdependent substratum surface characteristics of topography, surface chemistry, and resultant wettability. The finding that nanotextured surfaces stimulated cell adhesion may be important in biomedical applications as nonbiological cell-stimulating cues.

Acknowledgment. This work was supported by The Pennsylvania State Tobacco Settlement Formula Fund, The Pennsylvania State University Materials Research Institute, NIH AG13087-10, and NIH EB002016-12.

References and Notes

(1) Pittenger, M. F.; Mackay, A. M.; Beck, S. C.; Jaiswal, R. K.; Douglas, R.; Mosca, J. D.; Moorman, M. A.; Simonetti, D. W.; Craig, S.; Marshak, D. R. *Science* **1999**, *284*, 143.
(2) McBeath, R.; Pirone, D. M.; Nelson, C. M.; Bhadriraju, K.; Chen, C. S. *Dev. Cell* **2004**, *6*, 483.
(3) Boyan, B. D.; Hummert, T. W.; Dean, D. D.; Schwartz, Z. *Biomaterials* **1996**, *17*, 137.
(4) Vogler, E. A. *J. Biomater. Sci., Polym. Ed.* **1999**, *10*, 1015.
(5) Anselme, K. *Biomaterials* **2000**, *21*, 667.
(6) Lim, J. Y.; Liu, X.; Vogler, E. A.; Donahue, H. J. *J. Biomed. Mater. Res.* **2004**, *68A*, 504.
(7) Lim, J. Y.; Donahue, H. J. *J. Musculoskelet. Neuronal Interact.* **2004**, *4*, 396.
(8) Lim, J. Y.; Taylor, A. F.; Li, Z.; Vogler, E. A.; Donahue, H. J. *Tissue Eng.* **2005**, *11*, 19.
(9) Kim, Y. S.; Lim, J. Y.; Donahue, H. J.; Lowe, T. L. *Tissue Eng.* **2005**, *11*, 30.
(10) Lim, J. Y.; Hansen, J. C.; Siedlecki, C. A.; Runt, J.; Donahue, H. J. *J. R. Soc. Interface* **2005**, *2*, 97.
(11) den Braber, E. T.; de Ruijter, J. E.; Smits, H. T. J.; Ginsel, L. A.; von Recum, A. F.; Jansen, J. A. *Biomaterials* **1996**, *17*, 1093.
(12) Nealey, P. F. *Biomaterials* **1999**, *20*, 573.
(13) Teixeira, A. I.; Abrams, G. A.; Bertics, P. J.; Murphy, C. J.; Nealey, P. F. *J. Cell Sci.* **2003**, *116*, 1881.
(14) Britland, S.; Morgan, H.; Wojiak-Stodart, B.; Riehle, M.; Curtis, A.; Wilkinson, C. *Exp. Cell Res.* **1996**, *228*, 313.
(15) Oakley, C.; Jaeger, A. F.; Brunette, D. M. *Exp. Cell Res.* **1997**, *234*, 413.
(16) Dalby, M. J.; Riehle, M. O.; Johnstone, H. J. H.; Affrossman, S.; Curtis, A. S. G. *Biomaterials* **2002**, *23*, 2945.
(17) Dalby, M. J.; Yarwood, S. J.; Riehle, M. O.; Johnstone, H. J. H.; Affrossman, S.; Curtis, A. S. G. *Exp. Cell Res.* **2002**, *276*, 1.
(18) Dalby, M. J.; Childs, S.; Riehle, M. O.; Johnstone, H. J. H.; Affrossman, S. *Biomaterials* **2003**, *24*, 927.
(19) Dalby, M. J.; Giannaras, D.; Riehle, M. O.; Gadegaard, N.; Affrossman, S.; Curtis, A. S. G. *Biomaterials* **2004**, *25*, 77.

(20) Dalby, M. J.; Riehle, M. O.; Johnstone, H. J. H.; Affrossman, S.; Curtis, A. S. G. *J. Biomed. Mater. Res*. **2003**, *67A*, 1025.
(21) Riehle, M. O.; Dalby, M. J.; Johnstone, H.; MacIntosh, A.; Affrossman, S. *Mater. Sci. Eng.* **2003**, *C23*, 337.
(22) Rice, J. M.; Hunt, J. A.; Gallagher, J. A.; Hanarp, P.; Sutherland, D. S.; Gold, J. *Biomaterials* **2003**, *24*, 4799.
(23) Dalby, M. J.; Gadegaard, N.; Riehle, M. O.; Wilkinson, C. D.; Curtis, A. S. G. *Int. J. Biochem. Cell Biol*. **2004**, *36*, 2005.
(24) Alberts, B.; Bray, D.; Lewis, J.; Raff, M.; Roberts, K.; Watson, J. D. *Molecular Biology of the Cell*, 3rd ed.; Garland Publishing: New York and London, 1994.
(25) Shirato, I.; Tomino, Y.; Koide, H.; Sakai, T. *Cell Tissue Res.* **1991**, *266*, 1.
(26) Curtis, A.; Wilkinson, C *Trends Biotechnol.* **2001**, *19*, 97.
(27) Wang, M.; Zhu, X.; Wang, S.; Zhang, L. *Polymer* **1999**, *40*, 7387.
(28) Hsu, S. H.; Tang, C. M.; Lin, C. C. *Biomaterials* **2004**, *25*, 5593.
(29) Beamson, G.; Briggs, D. *High-Resolution XPS of Organic Polymers-The Scienta ESCA300 Database*; John Wiley & Sons Ltd: New York, 1992; pp 11−17, 37−39, 72−73, and 136−137.
(30) Braun, R. M.; Blenkinsopp, P.; Mullock, S. J.; Corlett, C.; Willey, K. F.; Vickerman, J. C.; Winograd, N. *Rapid Commun. Mass Spectrom.* **1998**, *12*, 1246.
(31) Nordfors, D.; Nilsson, A.; Mårtensson, N.; Svensson, S.; Gelius, U. *J. Chem. Phys.* **1988**, *88*, 2630.
(32) Shard, A. G.; Volland, C.; Davies, M. C.; Kissel, T. *Macromolecules* **1996**, *29*, 748.
(33) Mahoney, C. M.; Roberson, S. V.; Gillen, G. *Anal. Chem.* **2004**, *76*, 3199.
(34) Liu, S.; Chan, C. M.; Weng, L. T.; Ming, J. *Anal. Chem.* **2004**, *76*, 5165.
(35) Affrossman, S.; Henn, G.; O'Neill, S. A.; Pethrick, R. A.; Stamm, M. *Macromolecules* **1996**, *29*, 5010.
(36) Walheim, S.; Boltau, M.; Mlynek, J.; Krausch, G.; Steiner, U. *Macromolecules* **1997**, *30*, 4995.
(37) Affrossman, S.; O'Neill, S. A.; Stamm, M. *Macromolecules* **1998**, *31*, 6280.
(38) Tanaka, K.; Takahara, A.; Kajiyama, T. *Macromolecules* **1998**, *31*, 863.
(39) Affrossman, S.; Jerome, R.; O'Neill, S. A.; Schmitt, T.; Stamm, M. *Colloid Polym. Sci.* **2000**, *278*, 993.
(40) Affrossman, S.; Stamm, M. *Colloid Polym. Sci.* **2000**, *278*, 888.
(41) Zhao, X.; Zhao, W.; Sokolov, J.; Rafailovich, M. H.; Schwarz, S. A.; Wilkens, B. J.; Jones, R. A. L.; Kramer, E. J. *Macromolecules* **1991**, *24*, 5991.
(42) Tanaka, K.; Yoon, J. S.; Takahara, A.; Kajiyama, T. *Macromolecules* **1995**, *28*, 934.
(43) Raczkowska, J.; Bernasik, A.; Budkowski, A.; Sajewicz, K.; Penc, B.; Lekki, J.; Lekka, M.; Rysz, J.; Kowalski, K.; Czuba, P. *Macromolecules* **2004**, *37*, 7308.
(44) Owens, D. K.; Wendt, R. C. *J. Appl. Polym. Sci.* **1969**, *13*, 1741.
(45) Berlinger, A.; Gliemann, H.; Barczewski, M.; Durigon, P. E. R.; Petri, D. F. S.; Schimmel, T. *Surf. Interface Anal.* **2001**, *32*, 144.
(46) Mendelsohn, J. D.; Yang, S. Y.; Hiller, J.; Hochbaum, A. I.; Rubner, M. F.; *Biomacromolecules* **2003**, *4*, 96.
(47) Iwata, R.; Suk-In, P.; Hoven, V. P.; Takahara, A.; Akiyoshi, K.; Iwasaki, Y.; *Biomacromolecules* **2004**, *5*, 2308.
(48) Heilshorn, S. C.; Liu, J. C.; Tirrell, D. A.; *Biomacromolecules* **2005**, *6*, 318.

BM0503423